Revealing the Negative Capacitance Effect in Silicon Quantum Dot Light-Emitting Diodes via Temperature-Dependent Capacitance-Voltage Characterization

J. Mock, M. Kallergi, E. Groß, M. Golibrzuch, B. Rieger, and M. Becherer, *Member, IEEE*

***Abstract*—In this study, quantum dot light-emitting diodes based on non-toxic silicon quantum dots functionalized with hexyl and dodecyl organic ligands showed a negative capacitance effect. Current density-voltage ($J-V$) measurements revealed the charge transport mechanisms in the QLEDs. The capacitance-voltage ($C-V$) characteristics were measured with an LCR meter over a wide range of frequencies (200 Hz to 1 MHz) and at temperatures from $-40\,^{\circ}\mathrm{C}$ to $60\,^{\circ}\mathrm{C}$. The classical heterojunction theory can describe the operation of quantum LEDs, but an effect not predicted by Shockley's theory was observed. Negative capacitance values were recorded in both fabricated LEDs, which were not observed in SiQD-LEDs before. Hence, we investigate the negative capacitance origin and its influence on the device performance. We attribute the negative capacitance to trap-mediated recombination, where charges at defect sub-bandgap states contribute to the recombination but cannot be replenished fast enough. As a result, a current flows to re-establish the equilibrium, which lags behind the applied voltage, and the NC appears. By comparing the two functionalizations, we also observed a different temperature dependence of the positive capacitance peak and a stronger negative capacitance effect for dodecyl functionalized SiQDs. This effect is attributed to their improved charge carrier confinement abilities.**

***Index Terms*—Silicon quantum dot (SiQD), light-emitting diode (LED), negative capacitance (NC).**

I. Introduction

QUANTUM dot light-emitting diodes (QLEDs) are highly researched as promising electroluminescence (EL) devices. QDs itself combine the advantages of inorganic and organic materials by offering size-tunable emission [1], high color purity [2], easy processibility [3], and high photoluminescence quantum efficiency [4]. Additionally, QLEDs are expected to have improved stability compared to OLEDs because of their inorganic crystalline materials [5].

Many conventional QDs consist of toxic or heavy metal materials, such as Cd or Pb, and therefore, alternative materials are researched. A promising alternative is nanosized silicon, called silicon quantum dots (SiQDs) because of the non-toxicity of Si and its abundance in nature [6]. Even though Si is an indirect semiconductor, the quantum confinement effect leads to electroluminescence (EL) at sizes below the Bohr exciton radius of $4.5\,\mathrm{nm}$ [7]. By controlling the size and surface functionalization of the SiQDs, the emission wavelength for EL can be tuned [8], [9].

SiQD-LEDs reach already efficiencies of up to $8.6\,\%$ [10]. For further improvement, more information about the working mechanism in SiQD-LEDs is needed. The electrical characteristics of an LED can be described by using Shockley's classical pn junction theory [11]. To uncover the effect of charge transport on the capacity behavior of the SiQD-LEDs, capacitance-voltage ($C-V$) measurements are needed. $C-V$ measurement is a powerful technique where an AC signal is superimposed on a DC bias and the electrical capacitance and conductance response of the device can be recorded as a function of the applied AC frequency [12]–[14]. Charge injection and kinetics can be studied in a non-destructive manner [15]–[17] and processes that occur at various time scales can be monitored with high sensitivity [18]–[20].

We found a negative capacitance response in SiQD-LEDs. In many other optoelectronic devices such as GaAsP LEDs [21], metal-semiconductor Schottky diodes [22], OLEDs [23], p-i-n structures [24], or quantum well infrared detectors [21], a negative capacitance (NC) has been observed previously [14], [25]. A negative capacitance is not predicted by Shockley's theory, which only describes increasing diffusion capacitance [26]. NC was therefore attributed to parasitic inductance due to instrumental problems or false equipment calibration [13], [14], [21]. Capacitance measurements can, however, reproduce the NC effect, which would not be possible if it was a measurement artifact [21]. That brings us to the question of where the

Manuscript received 12 May 2022; revised 6 June 2022; accepted 15 June 2022. Date of publication 20 June 2022; date of current version 4 July 2022. This work was supported in part by Deutsche Forschungsgemeinschaft (DFG, German Research Foundation), under Project 245845833 within the International Research Training Group IRTG 2022, Alberta Technical University of Munich School for Functional Hybrid Materials (ATUMS). *(Corresponding authors: J. Mock; M. Becherer.)*

J. Mock, M. Kallergi, M. Golibrzuch, and M. Becherer are with the Department of Electrical and Computer Engineering, Technical University of Munich, 80333 Munich, Germany (e-mail: josef.mock@tum.de; maira.kallergi@tum.de; matthias.golibrzuch@tum.de; markus.becherer@tum.de).

E. Groß and B. Rieger are with the Department of Chemistry, Technical University of Munich, 85748 Garching, Germany (e-mail: elisabeth.gross@tum.de; rieger@tum.de).

This article has supplementary downloadable material available at https://doi.org/10.1109/JPHOT.2022.3184401, provided by the authors.

Digital Object Identifier 10.1109/JPHOT.2022.3184401

reproducible NC measurements in the SiQD-LEDs have their origin.

Still up to today, NC behavior in LEDs is controversially discussed and many different theories have been developed to explain it. In principle, NC can be described as a lag of current behind the voltage as the bias changes [14], [22]. This happens due to the faster consumption of free charge carriers than their replenishment and the induced compensatory current, which lags behind the voltage and tries to establish equilibrium [27]. Mathematically, this is expressed as a positive-valued time derivative of the transient current response to a voltage step [14], [28]. Changes in the capacitance signal reveal changes in the carrier and the trap state density, leading to negative capacitance in QD devices [28]. Bisquert *et al.* explain the NC via an electron injection model through interfacial states in OLEDs [23]. Others have attributed the effect to high-level injection [21], conductivity modulation, minority carrier injection, slow transient time of injected carriers, or charge trapping [22], [24], [25]. Bimolecular recombination, self-heating, and energetic disorder have also been considered as responsible mechanisms [20].

Capacitance-voltage measurements are crucial to understand the negative capacitance effect as the phenomenon is not fully understood. In particular, its behavior at different temperature and frequency modulations is important [11], [29].

In this contribution, we provide a comprehensive study of the capacitance characteristics of hexyl functionalized SiQD-LEDs. In doing so, we found an NC in SiQD-LEDs for the first time. To uncover the NC effect in SiQD-LEDs, we performed capacitance measurements for changing voltages and frequencies over a temperature range of $100\,^{\circ}\mathrm{C}$. We use the existing demarcation energy theory to explain the NC appearance. In order to improve the understanding of the effect, a second functionalization with a dodecyl chain was investigated because surface groups are known to influence the performance of SiQD-LEDs [30]. Our results offer additional information to uncover the effect of charge transport on the negative capacitance behavior in SiQD-LEDs.

II. Experimental Details

Device fabrication: The SiQD-LED consists of stacked layers from ITO ($120\,\mathrm{nm}$), PEDOT:PSS ($20\,\mathrm{nm}$), Poly-TPD ($10\,\mathrm{nm}$), SiQDs ($35\,\mathrm{nm}$), ZnO ($25\,\mathrm{nm}$), and Ag ($100\,\mathrm{nm}$) in that order. PEDOT:PSS solution (Ossila Al 4083, 1:3 in isopropanol, filtered through a $0.45\,\mu\mathrm{m}$ reactive cellulose filter) was spin coated onto the prestructured ITO substrates (Xinyan Technology, $15\,\Omega/\square$) with $50\,\mathrm{rps}$ and annealed at $140\,^{\circ}\mathrm{C}$ for $10\,\mathrm{min}$. Afterwards, the samples were immediately transferred to a nitrogen-filled glovebox (O_2 and $H_2O < 1\,\mathrm{ppm}$). Poly-TPD (Solaris Chem., $5\,\mathrm{mg/mL}$ in DCB) and SiQDs ($15\,\mathrm{mg/mL}$ in toluene) were spin coated with $67\,\mathrm{rps}$, and ZnO nanoparticles (InfinityPV, $1.8\,\mathrm{wt}\%$ in isopropanol) with $50\,\mathrm{rps}$. All layers were annealed at $140\,^{\circ}\mathrm{C}$ for $10\,\mathrm{min}$. The $100\,\mathrm{nm}$ silver electrode was thermally evaporated in a Univex 350 from Leybold ($3\,\mathrm{\AA/s}$, $\sim 8 \times 10^{-6}$ mbar).

Device characterization: All capacitance-voltage and photodiode measurements were performed inside a Vötsch VCL 4006 climatic chamber after a $15\,\mathrm{min}$ waiting period to let the samples adapt to the set temperature. For $C-V$ measurements an Agilent E4990 A LCR meter was used. An RMS value of $30\,\mathrm{mV}$ was set during all measurements to maintain the linearity of the response and to stay below the current limit of the LCR meter. The device irradiance was measured with a Thorlabs FDS10x10 photodiode. The LED was driven and measured by a Keithley 2602 A. The EL spectra of the LEDs were measured using a Thorlabs IS200-4 Integrating sphere and an AvaSpec-ULS2048x64TEC spectrometer from Avantes. The spectrometer was calibrated in the wavelength range of $350\,\mathrm{nm}$ to $1100\,\mathrm{nm}$ with an Avalight-HAL-CAL mini lamp from Avantes. All measurements were controlled with a Matlab program.

III. Results

The SiQD-LEDs used in this work are fabricated accordingly to the process described in our previous publication, hence extending the previous work [30]. To evaluate the negative capacitance effect in SiQD-LEDs, they are initially measured optoelectronically. The electrical $J(V)$ and capacitance characteristics $C(V_{\mathrm{bias}}, f, T)$ of a SiQD-LED with hexyl functionalization are measured to uncover the effect of charge transport on the capacitance behavior of the SiQD-LED. In Fig. 1 a) the current density is plotted, whereas the measured current is divided by the nominal LED area of $3\,\mathrm{mm} \times 3\,\mathrm{mm}$. It shows a gradual increase at the turn-on voltage followed by a steep increase with increasing applied voltages. The turn-on voltage is defined at an irradiance of $0.1\,\mu\mathrm{W\,cm^{-2}}$, where the electroluminescence can be detected without any error. The irradiance is shown in b) and shows an increase with voltages and flattens out at higher voltages. The resulting EQE defined as $EQE = \frac{N_{\mathrm{photons}}}{N_{\mathrm{electrons}}}$ is plotted over voltage in c). After a steep increase, it reaches a maximum with $0.73\,\%$ at around $2.9\,\mathrm{V}$ and decreases to about half the maximum value. In d), we measured the capacitance at $1\,\mathrm{kHz}$ and observed an NC, which had an unclear origin to us. In the following sections, we will discuss and explain the physical mechanisms behind the NC in our sample.

A. Negative Capacitance in SiQD-LEDs

In the capacitance measurement shown in Fig. 1 d) we see a small gradual increase of C up to a maximum point at around $2\,\mathrm{V}$. Above $2\,\mathrm{V}$ the capacitance decreases rapidly in magnitude and even reaches negative values from $2.8\,\mathrm{V}$ on. The highest magnitude of the NC is reached at ca. $3.4\,\mathrm{V}$ from where the magnitude becomes gradually smaller. The negative values of capacitance in Fig. 1 d) are however not predicted by the pn-junction theory, so there must be a different mechanism leading to the rapid disappearance of injected carriers. [11], [31] At the LED turn-on, the gradual increase is stopped and reverses until a steep decrease in capacity becomes visible. Finally, this ends in NC at the maximum EQE. The relationship between light emission, capacitance, and NC leads us to believe that e-h injection and recombination play a significant role in the NC appearance [25], [31], [32].

The physical concept of the demarcation energy can lead to NC. In this concept, electrons/holes in (deep) traps have a

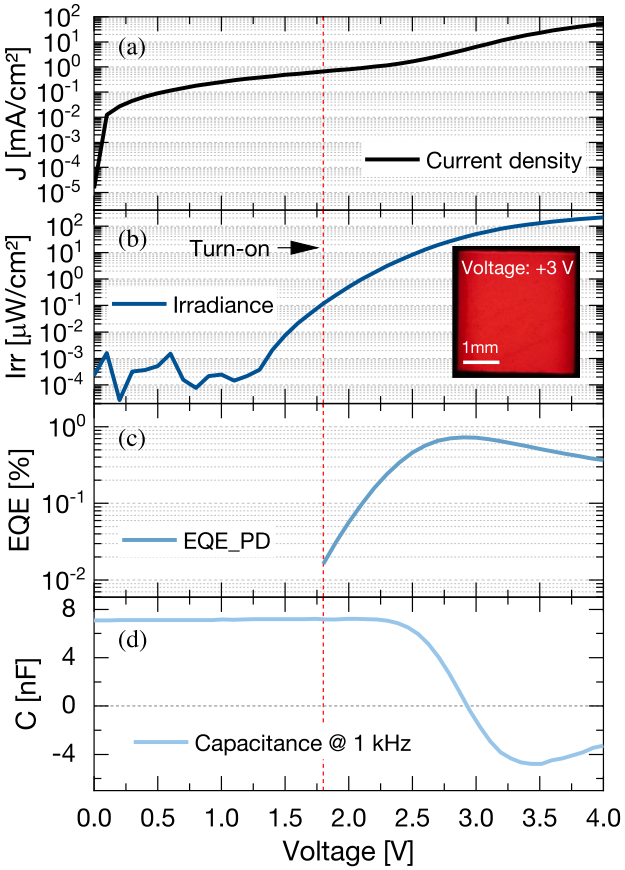

Fig. 1. a) $J-V$ characteristic of the hexyl functionalized SiQD-LED for positive bias. b) Irradiance of the SiQD-LED in log scale. The turn-on is defined at $0.1\,\mu$W cm^{-2}, which is indicated by the red dashed line in all plots. The microscope image shows the LED at an applied voltage of $+3$ V. c) EQE calculated from a) and b) shown in a log scale. d) Capacitance characteristic at 1 kHz at room temperature. The grey dashed line is indicating 0 nF.

finite probability of being thermally re-emitted into the conduction/valence band. The characteristic time scale τ_{trap} of this thermal emission or release from a trap energy level E_{trap} to the conduction band is given by [33]

$$\tau_{\text{trap}} = \gamma^{-1} exp\left(\frac{\Delta E}{k_{\text{B}}T}\right) \tag{1}$$

where ΔE is the energy difference of the trap energy level to the conduction/valence band ($|\Delta E| = |E_{\text{C,V}} - E_{\text{trap}}|$), γ the attempt-to-escape frequency with $\gamma = N_{\text{C,V}} v_{\text{th}} \sigma_{\text{n,p}}$, where $N_{\text{C,V}}$ is the conduction/valence band effective density of states, v_{th} the thermal velocity, and $\sigma_{\text{n,p}}$ the electron/hole capture cross section [34]–[37].

When an AC signal is applied in capacitance measurements, the AC frequency determines which trap levels can be probed. Thus, there is maximal frequency at which the defect states are still able to respond to the voltage modulation. The trap states need to fulfill the condition $\omega_{\text{AC}} = \tau_{\text{trap}}^{-1}$ with the angular frequency of the AC signal $\omega_{\text{AC}} = 2\pi f_{\text{AC}}$, while f_{AC} is the measurement frequency [34], [37]. From this condition, an energy level known as demarcation [34], [36], [38]–[41] can

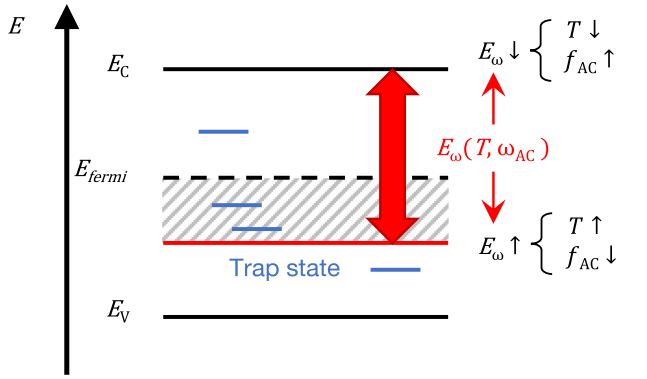

Fig. 2. Schematic representation of the band diagram to understand the demarcation energy effect. If the demarcation energy is large enough to cross the Fermi level, as shown here, trap states can be charged and discharged. The grey shaded area represents the energy area where trap states can be charged and discharged. The trapping and detrapping of charges results in a capacitance variation and can cause NC.

be determined by rearranging Eq. (1):

$$E_\omega = \Delta E = k_{\text{B}} T \ln\left(\frac{\gamma}{\omega_{\text{AC}}}\right) \tag{2}$$

This energy is also called cut-off [41], [42] or thermal activation energy [43], [44] but for the rest of this work, E_ω will be referred to as demarcation energy. A schematic representation of the demarcation energy is given in Fig. 2. It illustrates the band diagram with conduction and valence band, the fermi level E_{fermi}, and E_ω in red. Trapped charges whose energy levels lie above the red energy level and below the Fermi level will be able to contribute to the capacitance signal [13], [34], [36], [38], [42], [45]. This condition practically translates to the thermal emission rate $e_{\text{n,p}} = 1/\tau_{\text{trap}}$ being larger than the frequency of the AC signal, i.e. $e_{\text{n,p}} > \omega_{\text{AC}}$ [42], [46]. Traps energetically below E_ω will be "frozen" with respect to the AC signal since their capture and emission rates are lower than the modulating frequency [41], [47], [48]. The Fermi level that controls the state occupancy determines the upper energy limit, which traps contribute. States far above the Fermi level are empty and therefore cannot charge or discharge with the AC modulation, whereas charges in deep traps are also not probed since they are fully occupied. [49] So, only trapped charges that lie between the demarcation level and the Fermi level in the shaded area in Fig. 2 can produce an additional capacitance signal [38], [50]. As the Fermi level position moves with the AC modulation as an effect of barrier height modulation, traps can charge and discharge, resulting in a capacitance variation [22]. Furthermore, the same combination of (ω, T) might probe different energies for different traps [42].

The effect of NC in Fig. 1(d)) can be explained under the assumption of the demarcation energy. At low forward bias, holes and electrons are slowly injected in the device and start to accumulate at the interfacial layers, i.e. at the hole blocking layer (HBL) and electron blocking layer (EBL) respectively, as shown in the energy diagram in Fig. 3. The HOMO and LUMO levels are either from literature or directly from the manufacturer. [51]–[53] The EBL Poly-TPD with its deep HOMO

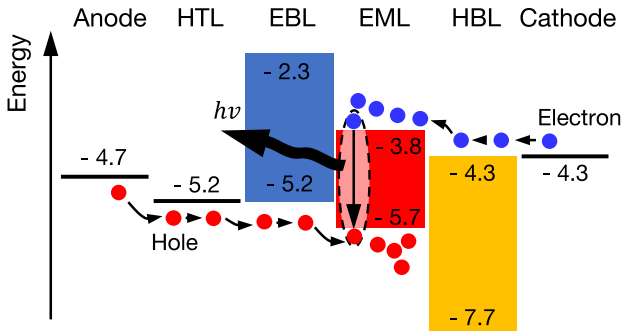

Fig. 3. Proposed energy diagram of the SiQD-LED with the path illustrated for electrons (blue) and holes (red) after injection from the electrodes. They accumulate at the interface between the EML (SiQDs) and the HBL (ZnO) and EBL (Poly-TPD), respectively. Electrons and holes recombine under the emission of a photon. The numbers at each layer give the highest occupied molecular orbital (HOMO) and lowest unoccupied molecular orbital (LUMO) energies.

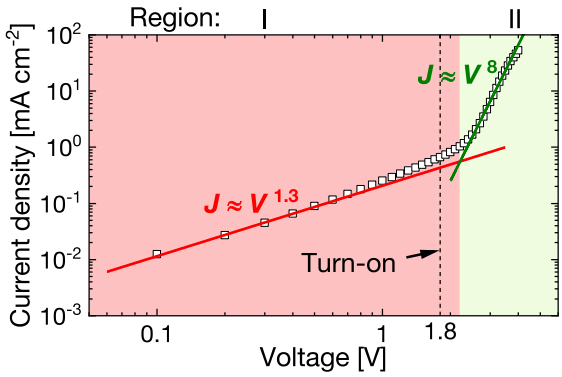

Fig. 4. Logarithmic representation of $J-V$ characteristics of SiQD-Hex LEDs. The colored lines are a linear fit to the measurement data. The hexyl sample shows two distinct regimes I and II which are highlighted in red and green background color, respectively. Ohmic transport in region I and space charge limited current with traps in region II.

and the high hole mobility of $\mu_h = 2.1 \times 10^{-3}$ cm^2 V^{-1} s^{-1} to 10^{-4} cm^2 V^{-1} s^{-1} is ideal for hole transport, while the low LUMO energy can efficiently block electrons. [52], [54], [55] On the other side of the EML, the HBL ZnO exhibits a high electron mobility ($\sim 2 \times 10^{-3}$ cm^2 V^{-1} s^{-1}) for electron transport and efficient hole blocking [56], [57]. Trapped carriers are also being re-emitted to the conduction band, contributing to the free charge distribution, thus increasing capacitance. As the turn-on voltage (red line in Fig. 1) of the device is reached, carriers recombine radiatively in the emissive layer (EML), including charges emitted from trap levels that are consumed irreversibly [27], [58]. At the end of one modulation cycle, the equilibrium defect population is disturbed as equilibrium lags behind the voltage, resulting in negative capacitance. A compensatory current is then induced to re-establish the equilibrium and the NC magnitude is decreasing again. So the responsible mechanism for NC is trap-mediated recombination [18], [20], [59], [60], where the charge carrier consumption rate is faster than the replenishment rate of the charge carriers [13], [18], [19], [25], [29], [31], [61].

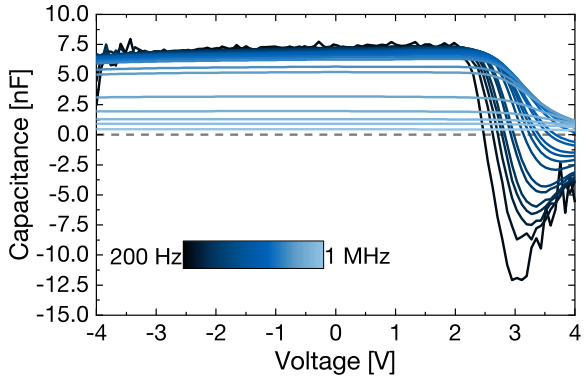

Fig. 5. $C-V$ characteristics of the SiQD-Hex LED probed at different AC signal frequencies from 200 Hz to 1 MHz. The phenomenon of negative capacitance is observed at the onset of recombination at around 2 V. As the frequency increases, the positive peak decreases. At the same time, the negative capacitance magnitude decreases, and the curve shifts to higher voltages.

B. Evidence of Trap States in the SiQD-LEDs

SiQDs are known to have high trap densities as they are not fully crystalline. Around a Si core, SiQDs exhibit a non-crystalline surface shell which is more prone to defects hence trap states [62]. We performed a reverse sweep of the voltage consecutive to the forward sweep (Fig. 1 a)) and a shift of the zero crossing is observed. This hysteretic behavior can be attributed to the presence of slowly responding traps in the system and is shown in SI Figure 1 [63], [64]. To further investigate, we analyze the $J-V$ measurement in a log-log scale in Fig. 4 because we expect space charge limited current transport (SCLC) as seen previously by Pfähler *et al.* [65] for SiQDs which confirms the presence of traps. Two linear regimes are identified in the measurement of the SiQD-Hex sample. At low voltages (red region), the graph can be described with ohmic behavior since J rises almost linearly with voltage. The slight deviation of the slope from unity is attributed to the shape of the density-of-states (DOS) distribution [66]. The green highlighted second regime can be characterized by a power law dependence ($J \propto V^m$, $m > 2$), which is attributed to the presence of exponentially distributed trap energy states [67]–[70]. This current transport is called trap-assisted space charge limited current, where the injected charge is larger than the intrinsic charge and traps affect the charge transport. The large exponent of $m = 8$ is similar ranges to Pfähler *et al.* [65] who measured SiQDs in nanogap electrodes and presented a detailed investigation of the charge transport in SiQDs. We considered their similar fitting results to our $J-V$ curve as confirmation for trap states in the SiQD-LEDs. Previously reported mobility values for SiQDs capped with allylbenzene are 6.5×10^{-6} cm^2 V^{-1} s^{-1} [71].

C. C-V Measurement Results

As we presented before, the demarcation energy equation is dependent on the frequency and temperature. Therefore, we investigate the capacitance of the hexyl functionalized LEDs for bias voltages of -4 V to 4 V for a range of frequencies (200 Hz - 1 MHz) followed by the same measurements at different temperatures ($-40\,^\circ$C to $60\,^\circ$C) to validate the theory.

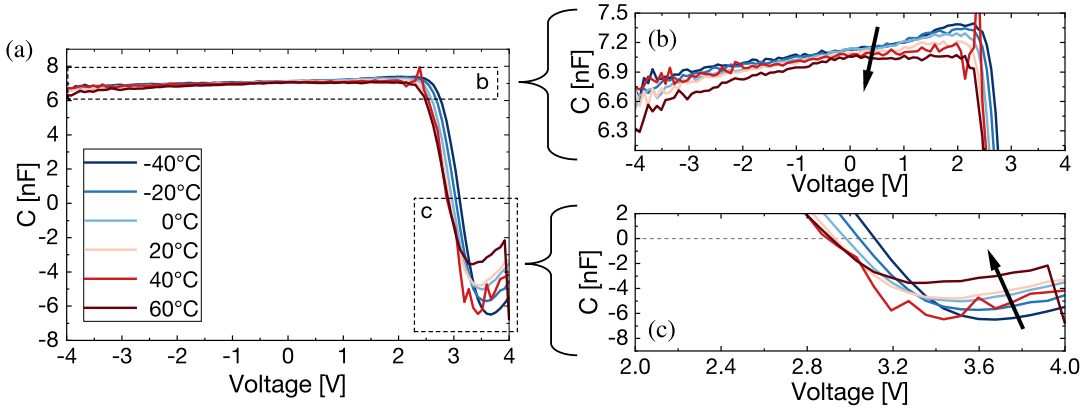

Fig. 6. (a) $C-V$ characteristics of the SiQD-Hex LED probed at different temperatures and fixed AC signal frequency of 1 kHz. (b) Zoom-in to the positive peak reduction of the capacitance. (c) Zoom-in to the NC, which becomes also smaller in magnitude with increasing temperature. The gray line indicates 0 nF. The phenomenon of accumulation and negative capacitance is reduced at higher temperatures. This can be attributed to increased carrier thermal escape with higher temperatures.

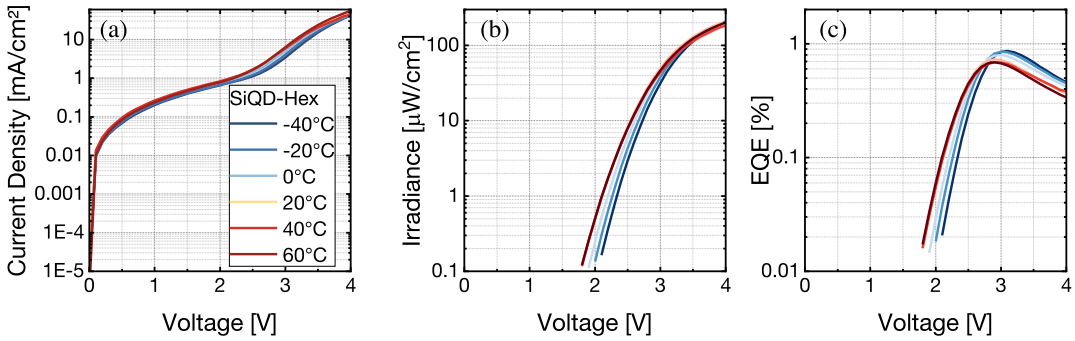

Fig. 7. (a) $J-V$ characteristic of hexyl LED for all temperatures. The legend applies to all other plots in this figure. (b) Irradiance and (c) EQE dependence. For low temperatures, the irradiance is lower but the EQE is increased.

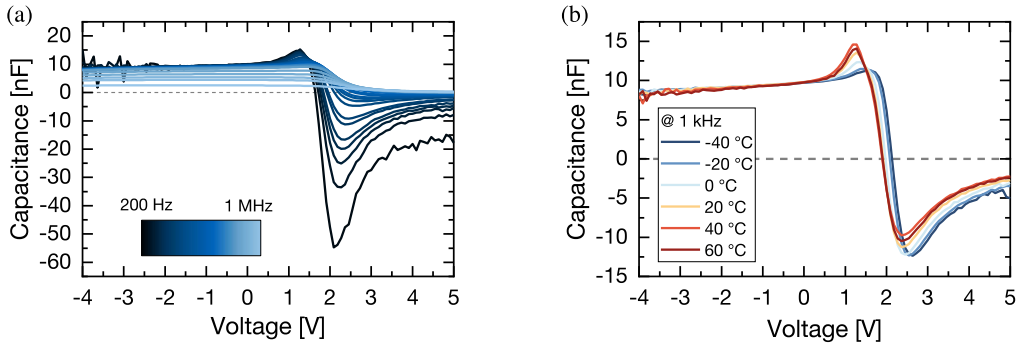

Fig. 8. (a) $C-V$ curve of the dodecyl sample at 20 °C for frequencies from 200 Hz up to 1 MHz. The phenomenon of negative capacitance is observed at the onset of recombination. As the frequency increases, the positive and negative capacitance decrease, and the curve shifts to higher voltages. (b) $C-V$ characteristics of the SiQD-Dodec sample probed at different temperatures at a frequency of 1 kHz. The positive capacitance peak increases as the temperature increases, while the magnitude of the negative capacitance decreases. The curve is also shifted to lower voltages with higher temperatures.

1) CV Frequency Sweep: In Fig. 5 we measured the capacitance in the range of -4 V to 4 V for frequencies from 200 Hz up to 1 MHz to investigate the frequency influence on the NC. The capacitance remains almost constant in reverse bias and low bias, until the turn-on voltage of around 2 V. Above the turn-on voltage, the capacitance decreases rapidly and becomes negative until a negative maximum at 3 V is reached, after which the capacitance becomes more positive. From a basic electrical perspective, NC can be described as an inductance-like behavior. However, NC cannot be treated as a classical inductance [25]. If that were the case, NC would increase with frequency and a magnetic field would also be observed [14], [28]. However, we did not observe an NC increase with frequency in our sample. Varying the frequency of the modulation voltage allows probing the device at different demarcation energies [39]. As the frequency increases in Fig. 5, the demarcation energy decreases, and the slowly responding traps are consequently frozen out because they cannot follow the increasing AC signal. The amount

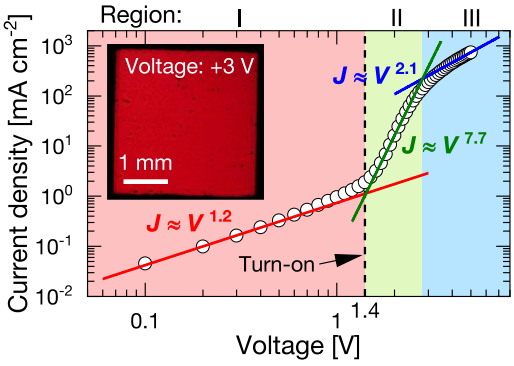

Fig. 9. Double logarithmic plot of the $J - V$ curve for the dodecene LED. The colored lines are a linear fit to the measurement data. Three regions represents different charge transport mechanisms that are highlighted with color. Region I in red, represents the ohmic behavior, region II in green the SCLC regime, and region III in blue shows the trap-free SCLC transport. The inset shows a microscope image of the dodecene LED at an applied bias of 3 V.

of thermally re-emitted charge carriers is reduced, thus less accumulation is observed, which corresponds to a decrease in the positive capacitance peak [43], [72]. Accordingly, less released carriers from trap states are consumed during recombination, a smaller compensatory current is required and NC reduces in magnitude at around 3 V. At high frequencies, trapping and detrapping occur rapidly, so a stationary accumulation of charges becomes difficult [28] and the re-establishment of equilibrium after recombination takes less time [58].

By increasing the frequency, we observe a shift of the curve towards higher voltages, which can also be explained via the demarcation energy. As the frequency is increased, E_ω is reduced and only shallow states can contribute to the capacitance signal. To compensate for the loss in the free carrier density due to freezing of deeper trap states, we need to increase the applied bias to reach the same free carrier density or capacitance value.

2) Temperature Sweep: The demarcation energy is dependent on both, frequency and temperature, as shown in Equation 2. Therefore, we have also varied the temperature to further test the demarcation energy theory. We performed the same capacitance measurements as before in a climatic chamber with temperatures ranging from $-40\,^\circ\mathrm{C}$ to $60\,^\circ\mathrm{C}$ in $20\,^\circ\mathrm{C}$ steps.

The results for the $C - V$ measurements of the SiQD-Hex sample at a probing frequency of 1 kHz are presented in Fig. 6. Three effects can be identified with the temperature change from $-40\,^\circ\mathrm{C}$ to $60\,^\circ\mathrm{C}$ as the temperature is increased: i) the positive maximum peak of the capacitance is decreasing ii) the magnitude of the NC is decreasing and iii) the $C - V$ curve shifts to lower voltages. As the temperature increases, E_ω in Eq. (2) increases as well and in our case, that means that deeper states contribute to the capacitance. With more free charge carriers in the system, the recombination is enhanced at a fixed rate, reducing the positive peak in Fig. 6 b) and the capacitance reaches negative values at lower voltages. The increasing temperature should also have a higher negative capacitance response, however, in our sample in Fig. 6 c), we see the opposite trend. This phenomenon can be explained if we consider other temperature-driven effects such as Poole-Frenkel emission. We assume that field-assisted escape processes of free charge carriers out of the quantum dots dominate over trap-mediated recombination. Therefore, the amount of charge carriers available for radiative recombination is reduced at higher voltages. As a result of increasing charge carrier escape, e-h recombination is reduced which leads to a decrease in the NC signal [25], [43].

3) Effect of Temperature on the SiQD-LED Performance: In the following, we present in Fig. 7 the temperature effect on the performance metrics of the SiQD-LEDs. We are doing this to check whether the behavior is consistent with the demarcation energy theory. For the $J - V$ characteristics in Fig. 7 a), we observe higher current densities with increasing temperatures because the thermal escape follows the Poole-Frenkel emission at high temperatures and high fields. [73] As a result, the irradiance is increased in b) because elevated temperatures enhance the charge carrier population while the recombination is faster in the SiQDs. [74] In Fig. 7 c), the EQE decreases with temperature. Since at higher temperatures (and high fields), the voltage modulated escape of charge carriers in the SiQDs is enhanced, it results in a ratio change of the $N_{\text{electrons}}$ and N_{photons} hence EQE decreases. As the thermal escape from the SiQDs is enhanced, radiative recombination becomes less efficient, so EQE declines. The curves in Fig. 7 a–c) shift towards lower voltages with increasing temperature, which coincides with the voltage shift of the $C - V$ curve for 1 kHz in the same direction as in SI Figure 2. This temperature behavior further supports our assumption that the NC is caused by charge injection and recombination effects. The temperature effect on the EL spectrum is plotted in SI Figure 3. It reveals that the EL spectrum is shifting with an increasing temperature towards a lower wavelength by 8 nm. Those findings match the previously reported temperature behavior, where the PL also blue shifts with decreasing temperature [74].

D. Dodecene Functionalization

To extend the assumption of a trap-assisted capacitance change via the demarcation energy, we prepared a SiQD-LED with a dodecene functionalization on the SiQDs. In our previous publication, [30] we showed that the organic ligand impacts the LED performance, thus, we wanted to see if it affects the demarcation energy in the capacitance measurements. The $C - V$ behavior in Fig. 8 a) reveals similar effects as the SiQD-Hex sample in the same frequency range. The curve shifts to higher voltages with increasing frequency, and the positive and negative capacitance reduces in magnitude. Both effects are in agreement with our presented theory.

The temperature-dependent capacitance curve at 1 kHz is displayed in Fig. 8b). By increasing the temperature, the NC peak shows the same trend as the hexyl functionalized SiQD-LED, it decreases and is also shifted to lower voltages. The trend of the positive capacitance, however, is reversed compared to the hexyl SiQD-LED. This discrepancy can be explained by comparing the properties of the two functionalizations. SiQD-LEDs with dodecyl chains show improved charge carrier localization due to a wider potential barrier, so the charge carrier

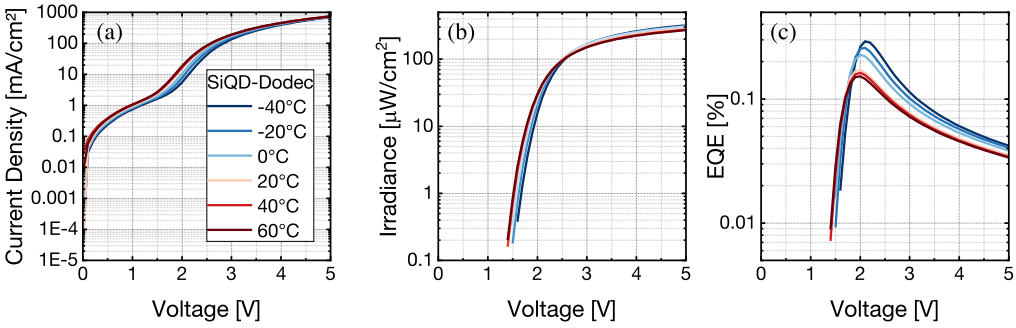

Fig. 10. Electrical characteristics of the SiQD-Dodec sample probed at different temperatures. The legend in (a) applies to all graphs in this figure. As the temperature increases, so does the current density in (a) and irradiance in (b) at a given voltage. At a crossover voltage of ≈2.6 V, the irradiance behavior reverses and decreases with increasing temperature. The same effect was also observed for the EQE in (c).

tunneling probability is reduced [30]. Since charges are more localized, increased temperature leads to more participation of trap states that increased charge accumulation due to an bigger demarcation energy [28], [75]. In contrast to the hexyl sample, the accumulated charge carriers can not recombine right away because an opposite charge because the potential barrier is missing. The bigger barrier prevents charges from reaching or leaving the SiQDs, thus increasing the positive capacitance with temperature. Besides, the capacitance peak occurs at lower applied voltages, where the field-assisted escape effect is smaller compared to the hexyl SiQD-LED.

Comparable to the Hex-sample, we investigated the $J-V$ log-log plot for the dodecene sample, shown in Fig. 9. The curve shows three regions instead of the two regions for the Hex-LED. The red ohmic region and the trap-assisted region with $m = 7.7$ are similar to the hexyl sample. Afterwards, the curve's fitting exponent decreases towards $m = 2.1$ in the blue region. The exponent $m = 2.1$ indicates the beginning of trap-free SCLC following the Mott-Gurney law [65]. The gradual transition between the SCLC with traps and the trap-free region is an indication of an energetic distribution of trap energies [76]. The dodecene sample has a current density one order of magnitude higher than the Hex sample due to increased pinholes, depicted in the inset in Fig. 9. Thus the trap states are filled up faster, and the trap free SCLC regime is reached.

The electrical behavior of the SiQD-Dodec LED in Fig. 10 shows a current density increase with temperature, accordingly to the SiQD-Hex LED. A more pronounced effect is seen in the irradiance and EQE. At 2.6 V the temperature dependence reverses and lower temperatures result in higher irradiance. 2.6 V is also the voltage at which the gradual current transport transitions from SCLC with traps to pure SCLC occurs. This crossover indicates that even more charges are injected into the active area (Fig. 10 b). Afterwards, the device efficiency decreases and can be attributed to increased non-radiative recombination [28].

E. Comparison of the Hexyl and Dodecene Capacitance Curves

In Fig. 11 a) the capacitance characteristics of both SiQD-Hex and SiQD-Dodec LEDs are plotted after normalizing them to their capacitance value at -4 V. We observe that the onset of the NC is at different bias values due to the different current driven through both LEDs. The magnitude of the positive and negative capacitance peaks in the SiQD-Dodec LED is larger compared to the Hex-LED. The dodecene SiQDs confines charges more efficiently impeding the transport of carriers to the next SiQD, so positive capacitance builds up more [28]. This increased accumulation combined with longer recombination lifetimes leads to a larger NC [26]. In Fig. 11 b), dC/dV is plotted on the same voltage scale. The bigger negative peak of the dodecene sample suggests a faster capacitance decay, thus a higher charge carrier consumption.

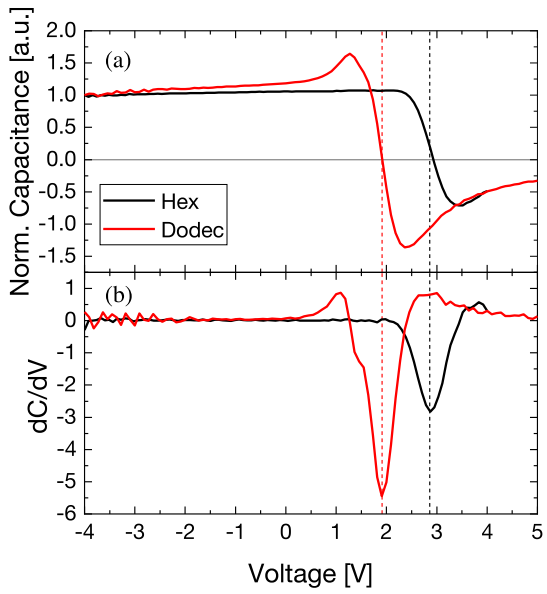

Fig. 11. (a) Normalized capacitance of the SiQD-Hex and SiQD-Dodec LED. In the case of dodecyl, more accumulation and larger magnitude of negative capacitance is observed at a lower voltage. (b) First derivative of the normalized capacitance.

IV. Conclusion

The effect of negative capacitance was presented for the first time in SiQD-LEDs with hexyl and dodecyl functionalized SiQDs. By analyzing the $J-V$ and $C-V$ measurements for

temperature ranges of $-40\,^{\circ}\mathrm{C}$ to $60\,^{\circ}\mathrm{C}$, the negative capacitance effect was fit into the existing demarcation energy formalism. When an increasing bias is applied to the LED and the turn-on voltage is reached, the consumption of carriers due to recombination is faster than carrier replenishment and a negative capacitance appears. With an increase in modulation frequency, deeper trapped charges cannot follow the AC signal and the negative capacitance value decreases. The demarcation energy is temperature-sensitive and for the SiQD-Hex sample, the accumulation of charge carriers was decreased with increasing temperature, whereas for the dodecene sample, more accumulation was observed. The different behavior for the accumulation peak is attributed to the better localization properties of the dodecyl functionalization. In both cases, the NC peak decreased in magnitude with increasing temperature. Our findings strongly indicate the demarcation energy as the physical mechanism for the appearance of NC in SiQD-LEDs.

The results are most likely valid for a wide range of quantum dot LEDs, as the organic ligand structure is present in many QD devices. Nevertheless, more surface functionalizations can be tested as they are easy to tailor to serve a specific purpose in QLEDs.

ACKNOWLEDGMENT

The authors acknowledge the support of the Central Electronics and Information Technology Laboratory – ZEIT$^{\mathrm{lab}}$.

REFERENCES

[1] C. B. Murray, C. R. Kagan, and M. G. Bawendi, "Synthesis and characterization of monodisperse nanocrystals and close-packed nanocrystal assemblies," *Annu. Rev. Mater. Sci.*, vol. 30, no. 1, pp. 545–610, 2000.

[2] S. Coe-Sullivan, J. S. Steckel, W.-K. Woo, M. G. Bawendi, and V. Bulović, "Large-area ordered quantum-dot monolayers via phase separation during spin-casting," *Adv. Funct. Mater.*, vol. 15, no. 7, pp. 1117–1124, 2005.

[3] P. Kathirgamanathan, L. M. Bushby, M. Kumaraverl, S. Ravichandran, and S. Surendrakumar, "Electroluminescent organic and quantum dot leds: The state of the art," *J. Display Technol.*, vol. 11, no. 5, pp. 480–493, 2015.

[4] T. A. Pringle *et al.*, "Bright silicon nanocrystals from a liquid precursor: Quasi-direct recombination with high quantum yield," *ACS Nano*, vol. 14, no. 4, pp. 3858–3867, 2020.

[5] X. Dai *et al.*, "Solution-processed, high-performance light-emitting diodes based on quantum dots," *Nature*, vol. 515, no. 7525, pp. 96–99, 2014.

[6] H. Yamada and N. Shirahata, "Silicon quantum dot light emitting diode at 620 nm," *Micromachines*, vol. 10, no. 5, 2019, Art. no. 318.

[7] E. G. Barbagiovanni, D. J. Lockwood, P. J. Simpson, and L. V. Goncharova, "Quantum confinement in Si and Ge nanostructures," *J. Appl. Phys.*, vol. 111, no. 3, 2012, Art. no. 034307.

[8] M. Dasog, G. B. de los Reyes, L. V. Titova, F. A. Hegmann, and J. G. C. Veinot, "Size vs surface: Tuning the photoluminescence of freestanding silicon nanocrystals across the visible spectrum via surface groups," *ACS Nano*, vol. 8, no. 9, pp. 9636–9648, 2014. [Online]. Available: https://pubs.acs.org/doi/10.1021/nn504109a

[9] F. Maier-Flaig *et al.*, "Multicolor silicon light-emitting diodes (SiLEDs)," *Nano Lett.*, vol. 13, no. 2, pp. 475–480, 2013. [Online]. Available: https://pubs.acs.org/doi/10.1021/nl3038689

[10] K.-Y. Cheng, R. Anthony, U. R. Kortshagen, and R. J. Holmes, "High-efficiency silicon nanocrystal light-emitting devices," *Nano Lett.*, vol. 11, no. 5, pp. 1952–1956, 2011.

[11] V. D. Trong, C. T. Anh, N. D. Cuong, P. H. Binh, C. T. Truong, and A. T. Pham, "Frequency dependence of negative capacitance in light-emitting devices," in *Proc. 4th Int. Conf. Commun. Electron.* Piscataway NJ, USA, 2012, pp. 44–47.

[12] H. F. Haneef, A. M. Zeidell, and O. D. Jurchescu, "Charge carrier traps in organic semiconductors: A review on the underlying physics and impact on electronic devices," *J. Mater. Chem. C*, vol. 8, no. 3, pp. 759–787, 2020.

[13] K. Bansal, "Electrical and optical investigations of the condensed matter physics of junction diodes under charge carrier injection," Ph.D. dissertation, Dept. Phys., Indian Inst. Sci. Educ. Res., Pune, India, 2014.

[14] M. Ershov, H. C. Liu, L. Li, M. Buchanan, Z. R. Wasilewski, and A. K. Jonscher, "Negative capacitance effect in semiconductor devices," *IEEE Trans. Electron Devices*, vol. 45, no. 10, pp. 2196–2206, Oct. 1998.

[15] S. Nowy, W. Ren, A. Elschner, W. Lövenich, and W. Brütting, "Impedance spectroscopy as a probe for the degradation of organic light-emitting diodes," *J. Appl. Phys.*, vol. 107, no. 5, 2010, Art. no. 054501.

[16] K. M. Nimith, N. S. Sterin, P. P. Das, G. Umesh, and M. N. Satyanarayan, "Capacitance and impedance spectroscopy studies of polymer light emitting diodes based on meh-ppv:bt blends," *Synthetic Met.*, vol. 250, pp. 99–103, 2019.

[17] G. Zaiats, S. Ikeda, and P. V. Kamat, "Optimization of the electron transport layer in quantum dot light-emitting devices," *NPG Asia Mater.*, vol. 12, no. 1, pp. 1–6, 2020.

[18] E. Ehrenfreund, C. Lungenschmied, G. Dennler, H. Neugebauer, and N. S. Sariciftci, "Negative capacitance in organic semiconductor devices: Bipolar injection and charge recombination mechanism," *Appl. Phys. Lett.*, vol. 91, no. 1, 2007, Art. no. 012112.

[19] F. Ebadi, N. Taghavinia, R. Mohammadpour, A. Hagfeldt, and W. Tress, "Origin of apparent light-enhanced and negative capacitance in perovskite solar cells," *Nature Commun.*, vol. 10, no. 1, 2019, Art. no. 1574.

[20] Q. Niu, N. I. Crăciun, G.-J. A. H. Wetzelaer, and P. W. M. Blom, "Origin of negative capacitance in bipolar organic diodes," *Phys. Rev. Lett.*, vol. 120, no. 11, 2018, Art. no. 116602.

[21] L.-F. Feng, J. Wang, C.-Y. Zhu, H.-X. Cong, Y. Chen, and C.-D. Wang, "Experimental study of negative capacitance in leds," *Optoelectron. Lett.*, vol. 1, no. 2, pp. 124–126, 2005.

[22] A. G. U. Perera, W. Z. Shen, M. Ershov, H. C. Liu, M. Buchanan, and W. J. Schaff, "Negative capacitance of gaas homojunction far-infrared detectors," *Appl. Phys. Lett.*, vol. 74, no. 21, pp. 3167–3169, 1999.

[23] J. Bisquert, "A variable series resistance mechanism to explain the negative capacitance observed in impedance spectroscopy measurements of nanostructured solar cells," *Phys. Chem. Chem. Phys. : PCCP*, vol. 13, no. 10, pp. 4679–4685, 2011.

[24] L. S. C. Pingree, B. J. Scott, M. T. Russell, T. J. Marks, and M. C. Hersam, "Negative capacitance in organic light-emitting diodes," *Appl. Phys. Lett.*, vol. 86, no. 7, 2005, Art. no. 073509. [Online]. Available: https://aip.scitation.org/doi/full/10.1063/1.1865346

[25] E.-M. Bourim and J. in Han, "Size effect on negative capacitance at forward bias in InGaN/GaN multiple quantum well-based blue led," *Electron. Mater. Lett.*, vol. 12, no. 1, pp. 67–75, 2016.

[26] L. Wang *et al.*, "Influence of carrier screening and band filling effects on efficiency droop of InGaN light emitting diodes," *Opt. Exp.*, vol. 19, no. 15, pp. 14182–14187, 2011.

[27] K. Bansal, M. Henini, M. S. Alshammari, and S. Datta, "Dynamics of electronic transitions and frequency dependence of negative capacitance in semiconductor diodes under high forward bias," *Appl. Phys. Lett.*, vol. 105, no. 12, 2014, Art. no. 123503.

[28] C. Blauth, P. Mulvaney, and T. Hirai, "Negative capacitance as a diagnostic tool for recombination in purple quantum dot leds," *J. Appl. Phys.*, vol. 125, no. 19, 2019, Art. no. 195501.

[29] M. Guan, L. Niu, Y. Zhang, X. Liu, Y. Li, and Y. Zeng, "Space charges and negative capacitance effect in organic light-emitting diodes by transient current response analysis," *RSC Adv.*, vol. 7, no. 80, pp. 50598–50602, 2017.

[30] J. Mock, E. Groß, M. J. Kloberg, B. Rieger, and M. Becherer, "Surface engineering of silicon quantum dots: Does the ligand length impact the optoelectronic properties of light–emitting diodes?," *Adv. Photon. Res.*, vol. 2, no. 9, 2021, Art. no. 2100083.

[31] L.-F. Feng, C.-Y. Zhu, Y. Chen, Z.-B. Zheng, and C.-D. Wang, "Mechanism of negative capacitance in LEDs," *Optoelectron. Lett.*, vol. 1, no. 2, pp. 127–130, 2005.

[32] G. Garcia-Belmonte, H. J. Bolink, and J. Bisquert, "Capacitance-voltage characteristics of organic light-emitting diodes varying the cathode metal: Implications for interfacial states," *Phys. Rev. B*, vol. 75, no. 8, 2007, Art. no. 085316.

[33] S. S. Hegedus and E. A. Fagen, "Midgap states in a –si:h and a –sige:h p – i – n solar cells and schottky junctions by capacitance techniques," *J. Appl. Phys.*, vol. 71, no. 12, pp. 5941–5951, 1992.

[34] L. Xu, J. Wang, and J. W. P. Hsu, "Transport effects on capacitance-frequency analysis for defect characterization in organic photovoltaic devices," *Phys. Rev. Appl.*, vol. 6, no. 6, 2016, Art. no. 064020.

[35] R. Herberholz, T. Walter, and H. W. Schock, "Density of states in cuin$(SSe)_2$ thin films from modulated photocurrent measurements," *J. Appl. Phys.*, vol. 76, no. 5, pp. 2904–2911, 1994.

[36] E. von Hauff, "Impedance spectroscopy for emerging photovoltaics," *J. Phys. Chem C*, vol. 123, no. 18, pp. 11329–11346, 2019.

[37] E. Kask, T. Raadik, M. Grossberg, R. Josepson, and J. Krustok, "Deep defects in Cu_2ZnSnS_4 monograin solar cells," *Energy Procedia*, vol. 10, pp. 261–265, 2011.

[38] J. A. Carr, "The identification and characterization of electronic defect bands in organic photovoltaic devices," Ph.D. dissertation, Dept. Elect. Eng., Iowa State Univ., Ames, IA, USA, 2014.

[39] P. P. Boix, G. Garcia-Belmonte, U. Muñecas, M. Neophytou, C. Waldauf, and R. Pacios, "Determination of gap defect states in organic bulk heterojunction solar cells from capacitance measurements," *Appl. Phys. Lett.*, vol. 95, no. 23, 2009, Art. no. 233302.

[40] T. Walter, R. Herberholz, C. Müller, and H. W. Schock, "Determination of defect distributions from admittance measurements and application to Cu(In,Ga)Se_2 based heterojunctions," *J. Appl. Phys.*, vol. 80, no. 8, pp. 4411–4420, 1996.

[41] M. Anutgan and I. Atilgan, "Forward bias capacitance spectroscopy for characterization of semiconductor junctions: Application to a-si:h p-i-n diode," *Appl. Phys. Lett.*, vol. 102, no. 15, 2013, Art. no. 153504.

[42] J. Heath and P. Zabierowski, "Capacitance spectroscopy of thin-film solar cells," in *Advanced Characterization Techniques for Thin Film Solar Cells*, D. Abou-Ras, T. Kirchartz, and U. Rau, Eds., Weinheim, Germany: Wiley-VCH Verlag GmbH & Co KGaA, 2016, pp. 93–119.

[43] K. Bansal and S. Datta, "Temperature dependent reversal of voltage modulated light emission and negative capacitance in algainp based multi quantum well light emitting devices," *Appl. Phys. Lett.*, vol. 102, no. 5, 2013, Art. no. 053508.

[44] E.-M. Bourim and J. in Han, "Electrical characterization and thermal admittance spectroscopy analysis of InGaN/GaN mqw blue led structure," *Electron. Mater. Lett.*, vol. 11, no. 6, pp. 982–992, 2015.

[45] O. A. Soltanovich and E. B. Yakimov, "Analysis of the temperature dependence of the capacitance-voltage characteristics of InGaN/GaN multiple quantum well light-emitting structures," *Semiconductors*, vol. 47, no. 1, pp. 162–168, 2013.

[46] G. L. Miller, D. V. Lang, and L. C. Kimerling, "Capacitance transient spectroscopy," *Annu. Rev. Mater. Sci.*, vol. 7, no. 1, pp. 377–448, 1977.

[47] O. Armbruster, C. Lungenschmied, and S. Bauer, "Investigation of trap states and mobility in organic semiconductor devices by dielectric spectroscopy: Oxygen-doped P3HT:PCBM solar cells," *Phys. Rev. B*, vol. 86, no. 23, 2012, Art. no. 235201.

[48] J. M. Montero, J. Bisquert, G. Garcia-Belmonte, H. J. Bolink, and E. M. Barea, "Interpretation of capacitance spectra and transit times of single carrier space-charge limited transport in organic layers with field-dependent mobility," *Physica Status Solidi (a)*, vol. 204, no. 7, pp. 2402–2410, 2007.

[49] N. D. Nguyen, M. Schmeits, and H. P. Loebl, "Determination of charge-carrier transport in organic devices by admittance spectroscopy: Application to hole mobility in α -NPD," *Phys. Rev. B*, vol. 75, no. 7, 2007, Art. no. 075307.

[50] T. Muntasir and S. Chaudhary, "Understanding defect distributions in polythiophenes via comparison of regioregular and regiorandom species," *J. Appl. Phys.*, vol. 118, no. 20, 2015, Art. no. 205504.

[51] A. Angı *et al.*, "The influence of surface functionalization methods on the performance of silicon nanocrystal leds," *Nanoscale*, vol. 10, no. 22, pp. 10337–10342, 2018. [Online]. Available: https://xlink.rsc.org/?DOI=C7NR09525B

[52] L. Lan *et al.*, "Preparation of efficient quantum dot light-emitting diodes by balancing charge injection and sensitizing emitting layer with phosphorescent dye," *J. Mater. Chem. C*, vol. 7, no. 19, pp. 5755–5763, 2019.

[53] B. J. Hopkins and J. C. Riviere, "Work function values from contact potential difference measurements," *Brit. J. Appl. Phys.*, vol. 15, no. 8, pp. 941–946, 1964. [Online]. Available: https://iopscience.iop.org/article/10.1088/0508-3443/15/8/309/meta

[54] W. W. Zhu, S. Xiao, and I. Shih, "Field-effect mobilities of polyhedral oligomeric silsesquioxanes anchored semiconducting polymers," *Appl. Surf. Sci.*, vol. 221, no. 1–4, pp. 358–363, 2004.

[55] Q. J. Sun, B. H. Fan, Z. A. Tan, C. H. Yang, Y. F. Li, and Y. Yang, "White light from polymer light-emitting diodes: Utilization of fluorenone defects and exciplex," *Appl. Phys. Lett.*, vol. 88, no. 16, 2006, Art. no. 163510.

[56] W. Gu *et al.*, "Silicon-quantum-dot light-emitting diodes with interlayer-enhanced hole transport," *IEEE Photon. J.*, vol. 9, no. 2, 2017, Art. no. 4500610. [Online]. Available: https://ieeexplore.ieee.org/document/7858634/

[57] S.-H. Liao, H.-J. Jhuo, Y.-S. Cheng, and S.-A. Chen, "Fullerene derivative-doped zinc oxide nanofilm as the cathode of inverted polymer solar cells with low-bandgap polymer (PTB7-Th) for high performance," *Adv. Mater.*, vol. 25, no. 34, pp. 4766–4771, 2013. [Online]. Available: https://doi.wiley.com/10.1002/adma.201301476

[58] K. Bansal and S. Datta, "Voltage modulated electro-luminescence spectroscopy to understand negative capacitance and the role of sub-bandgap states in light emitting devices," *J. Appl. Phys.*, vol. 110, no. 11, 2011, Art. no. 114509.

[59] C. Y. Zhu *et al.*, "Negative capacitance in light-emitting devices," *Solid-State Electron.*, vol. 53, no. 3, pp. 324–328, 2009.

[60] C. D. Wang, C. Y. Zhu, G. Y. Zhang, J. Shen, and L. Li, "Accurate electrical characterization of forward AC behavior of real semiconductor diode: Giant negative capacitance and nonlinear interfacial layer," *IEEE Trans. Electron Devices*, vol. 50, no. 4, pp. 1145–1148, Apr. 2003.

[61] N. C. Chen, P. Y. Wang, and J. F. Chen, "Low frequency negative capacitance behavior of molecular beam epitaxial gaas n-low temperature-i-p structure with low temperature layer grown at a low temperature," *Appl. Phys. Lett.*, vol. 72, no. 9, pp. 1081–1083, 1998.

[62] A. N. Thiessen *et al.*, "Silicon nanoparticles: Are they crystalline from the core to the surface?," *Chem. Mater.*, vol. 31, no. 3, pp. 678–688, 2019. [Online]. Available: https://pubs.acs.org/doi/10.1021/acs.chemmater.8b03074

[63] W. Brütting, H. Riel, T. Beierlein, and W. Riess, "Influence of trapped and interfacial charges in organic multilayer light-emitting devices," *J. Appl. Phys.*, vol. 89, no. 3, 2001, Art. no. 1704.

[64] P. H. Nguyen, S. Scheinert, S. Berleb, W. Brütting, and G. Paasch, "The influence of deep traps on transient current–voltage characteristics of organic light-emitting diodes," *Org. Electron.*, vol. 2, no. 3–4, pp. 105–120, 2001.

[65] S. Pfaehler, A. Angı, D. Chryssikos, A. Cattani-Scholz, B. Rieger, and M. Tornow, "Space charge-limited current transport in thin films of alkyl-functionalized silicon nanocrystals," *Nanotechnology*, vol. 30, no. 39, 2019, Art. no. 395201. [Online]. Available: https://iopscience.iop.org/article/10.1088/1361-6528/ab2c28

[66] G. A. H. Wetzelaer, M. Kuik, H. T. Nicolai, and P. W. M. Blom, "Trap-assisted and langevin-type recombination in organic light-emitting diodes," *Phys. Rev. B*, vol. 83, no. 16, 2011, Art. no. 165204.

[67] S. Diaham and M.-L. Locatelli, "Space-charge-limited currents in polyimide films," *Appl. Phys. Lett.*, vol. 101, no. 24, 2012, Art. no. 242905.

[68] A. S. Sarkar and S. K. Pal, "Exponentially distributed trap-controlled space charge limited conduction in graphene oxide films," *J. Phys. D: Appl. Phys.*, vol. 48, no. 44, 2015, Art. no. 445501.

[69] V. Coropceanu, J. Cornil, D. A. da Silva Filho, Y. Olivier, R. Silbey, and J.-L. Brédas, "Charge transport in organic semiconductors," *Chem. Rev.*, vol. 107, no. 4, pp. 926–952, 2007.

[70] M. A. Rafiq, "Carrier transport mechanisms in semiconductor nanostructures and devices," *J. Semicond.*, vol. 39, no. 6, 2018, Art. no. 061002.

[71] F. Maier-Flaig, "Silizium-nanokristalle für optoelektronische anwendungen," Ph.D. dissertation, Dept. Elect. Eng. Inf. Technol. Karlsruher Institut Für Technologie, Karlsruhe, Germany, 2013.

[72] P. Chattopadhyay and B. RayChaudhuri, "Frequency dependence of forward capacitance-voltage characteristics of Schottky barrier diodes," *Solid-State Electron.*, vol. 36, no. 4, pp. 605–610, 1993.

[73] S. M. Sze and K. N. Kwok, *Semiconductor Devices Physics and Technology*, 3rd ed., Hoboken, NJ, USA: Wiley, 2006. [Online]. Available: https://onlinelibrary.wiley.com/doi/book/10.1002/0470068329

[74] M. Jakob, M. Javadi, J. G. Veinot, A. Meldrum, A. Kartouzian, and U. K. Heiz, "Ensemble effects in the temperature-dependent photoluminescence of silicon nanocrystals," *Chem. - A. Eur. J.*, vol. 25, no. 12, pp. 3061–3067, 2019. [Online]. Available: https://chemistry-europe.onlinelibrary.wiley.com/doi/abs/10.1002/chem.201804986

[75] M. Zhang *et al.*, "Positive temperature dependence of the electroluminescent performance in a colloidal quantum dot light-emitting diode," *Dyes Pigments*, vol. 195, 2021, Art. no. 109703.

[76] P. Blom and M. de Jong, "Electrical characterization of polymer light-emitting diodes," *IEEE J. Sel. Topics Quantum Electron.*, vol. 4, no. 1, pp. 105–112, Jan./Feb. 1998.